Design of the first fusion experiment to achieve target energy gain math xmlns="http://www.w3.org/1998/Math/MathML">mrow>mi>G/mi>mo>>/mo>mn>1/mn>/mrow>/math>

A. L. Kritcher et al.

Phys. Rev. E **109**, 025204 — Published 5 February 2024

DOI: 10.1103/PhysRevE.109.025204

Design of the first fusion experiment to achieve target energy gain > 1

A. L. Kritcher,[1,*] A. B. Zylstra,[1] C. R. Weber,[1] O. A. Hurricane,[1] D. A. Callahan,[1,2] D. S. Clark,[1] L. Divol,[1] D. E. Hinkel,[1] K. Humbird,[1] O. Jones$^{\psi}$,[1] J. D. Lindl,[1] S. Maclaren,[1] D. J. Strozzi,[1] C. V. Young,[1] A. Allen,[3] B. Bachmann,[1] K. L. Baker,[1] T. Braun,[1] G. Brunton,[1] D. T. Casey,[1] T. Chapman,[1] C. Choate,[1] E. Dewald,[1] J.-M. G. Di Nicola,[1] M. J. Edwards,[1] S. Haan,[1] T. Fehrenbach,[4] M. Hohenberger,[1] E. Kur,[1] B. Kustowski,[1] C. Kong,[3] O. L. Landen,[1] D. Larson,[1] B. J. MacGowan,[1] M. Marinak,[1] M. Millot,[1] A. Nikroo,[1] R. Nora,[1] A. Pak,[1] P. K. Patel,[1,2] J. E. Ralph,[1] M. Ratledge,[3] M. S. Rubery,[1] D. J. Schlossberg,[1] S. M. Sepke,[1] M. Stadermann,[1] T. I. Suratwala,[1] R. Tommasini,[1] R. Town,[1] B. Woodworth,[1] B. Van Wonterghem,[1] and C. Wild[4]

[1]*Lawrence Livermore National Laboratory, P.O. Box 808, Livermore, California 94551-0808, USA*
[2]*now at Focused Energy Inc., 11525-B Stonehollow Drive, Suite 200, Austin TX 78758, USA*
[3]*General Atomics, San Diego, California 92186, USA*
[4]*Diamond Materials GMBH, 79108 Freiburg, Germany*

(Dated: January 3, 2024)

In this work we present the design of the first controlled fusion laboratory experiment to reach target gain >1 N221204 (Dec. 5^{th} 2022) [Phys. Rev. Lett. XX, YY (2023)], performed at the National Ignition Facility, where the fusion energy produced (3.15MJ) exceeded the amount of laser energy required to drive the target (2.05MJ). Following the demonstration of ignition according to the Lawson criterion N210808, experiments were impacted by non-ideal experimental fielding conditions, such as increased (known) target defects that seeded hydrodynamic instabilities or unintentional low mode asymmetries from non-uniformities in the target or laser delivery, which led to reduced fusion yields < 1 Megajoule. This letter details design changes, including using an extended higher energy laser pulse to drive a thicker high density carbon (HDC, aka "diamond") capsule, that led to increased fusion energy output compared to N210808 as well as improved robustness for achieving high fusion energies (>1 Megajoule) in the presence of significant low-mode asymmetries. For this design, the burn-up fraction of the DT fuel was increased (∼4% fuel burn-up and a target gain of ∼1.5 compared to ∼2% fuel burn-up and target gain ∼0.7 for N210808) as a result of increased total (DT + capsule) areal density at maximum compression compared to N210808. Radiation-hydrodynamic simulations of this design predicted achieving target gain >1 and also the magnitude of increase in fusion energy produced compared to N210808. The plasma conditions and hot spot power balance (fusion power produced vs input power and power losses) using these simulations are presented. Since the drafting of this manuscript, the results of this paper have been replicated and exceeded (N230729) in this design, together with a higher quality diamond capsule, setting a new record of ∼3.88 MJ of fusion energy and fusion energy target gain of ∼1.9.

INTRODUCTION

Fusion offers the promise of clean limitless energy, fueled by isotopes of Hydrogen, that could be the long-term answer to rapidly growing global energy demands, provide energy security in times of unforeseen political tension, and address climate changes from greenhouse gas emission. Generating more fusion energy than required to generate the fusion reactions has been a long standing goal of all fusion energy approaches, and the last remaining milestone for the National Ignition Facility (NIF) [1] to claim fusion "ignition" [2]. Ignition is a prerequisite for generating net energy gain in the inertial confinement fusion approach (ICF) [3, 4] and requires reaching extreme conditions (tens of millions of degrees and hundreds of billions of atmospheres) to overcome the electrostatic repulsion of Deuterium and Tritium (DT) and enable fusion to occur. Energy is released in the form of a Helium (α) particle and a more energetic neutron [D+T →n (14.1 MeV)+^{4}He (3.5 MeV)] [5]. These conditions are created by imploding DT fuel at extreme velocities to do mechanical work on a central plasma, or 'hot spot" made up of a small fraction of the initial fuel, using a higher density shock-compressed DT fuel piston [6]. High areal densities of the DT fuel in the "hot spot" and surrounding fuel piston are required for absorption of energetic α particles (^{4}He) born in the fusion process to heat the hot spot plasma ("self-heating") and for longer confinement times to enable more of the DT to fuse before the hot compressed fuel explodes under its own pressure and cools the plasma. If sufficient self-heating from absorption of the α particles occurs, the hot spot will ignite and create a burn wave that moves through the remaining cooler fuel piston, significantly increasing the energy output.

Ignition by Lawson criterion [7] was first demonstrated at the NIF on Aug. 8th 2021 [NIF shot No. N210808]

[1] $^{\psi}$Deceased

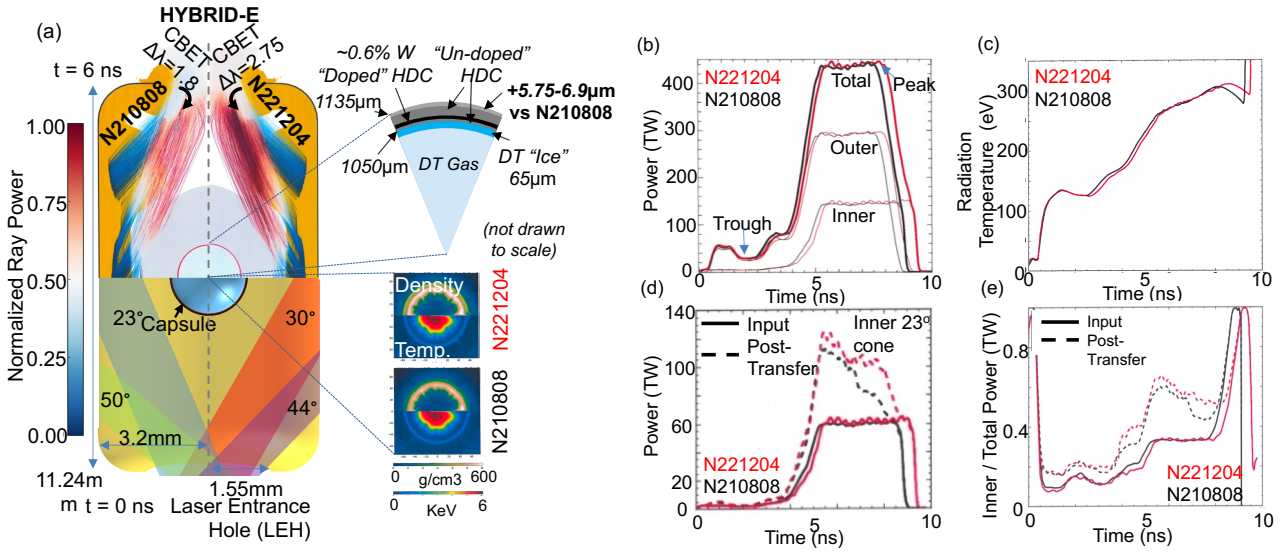

FIG. 1. (a) Schematic of the target configuration showing the hohlraum and spherical diamond capsule that contains DT fuel. Radiation hydrodynamics simulations of the integrated hohlraum and capsule (top) show the material positions and plasma filling into the hohlraum at time = 6 ns for N221204 (right) compared to N210808 (left). Also shown are simulated laser ray powers and an expanded view of the density and temperature at stagnation for N221204 vs N210808 from α-off simulations (simulations where α particle deposition is turned off). The radiation drive symmetry was controlled by transferring energy between laser beams through wavelength detuning ($\Delta\lambda$) and by precisely defining the balance of laser powers between the "inner" (23° & 30°) and "outer" (44° & 50°) beams throughout the duration of the laser pulse (b). The "Peak" of the laser power was extended by about 300ps to drive the thicker diamond capsule and the "trough" was lengthened to preserve the shock timing. (c) Simulated hohlraum internal radiation temperature ($T_{\rm rad}$) as a function of time shows the extended and higher radiation temperature for N221204 compared to N210808. The near vertical rise of the $T_{\rm rad}$ at the end of the drive for both cases is due to re-heating of the hohlraum from the capsule fusion output. (d) Calculated change in inner cone power (e.g. on the 23° cone) post-energy transfer. This amount of transfer was increased for N221204 (red) compared to N210808 (black) via increasing $\Delta\lambda$ from 1.8$\AA$ to 2.75$\AA$ to maintain symmetry with the longer laser pulse and thicker ablator. (e) Ratio of the full "inner" cone power to total laser power for the incident laser pulse (solid) and post-transfer pulse (dashed).

[8–10] by optimizing the implosion design and increasing the energy-density of the hot spot, as well as the target quality (the diamond capsule that holds the DT fuel). While achieving ignition by Lawson Criterion, N210808 only produced ~70% of the laser energy required to drive the experiment as fusion energy. In addition, follow-on experiments showed variability to non-ideal experimental fielding conditions that lowered the performance to 30-50% that of N210808. These perturbations include unintentional low mode asymmetries and hydrodynamic instabilities seeded by compromised diamond capsule quality that caused mixing of high-Z material into the hot spot plasma.

This work presents the first fusion design to ever produce more fusion energy than energy delivered to the target, or target gain greater than one, in a laboratory setting, and is the current record holder for fusion energy produced at the NIF (3.88 MJ and target gain of ~1.5-1.9x). Also see the accompanying papers which describe the experimental results (Pak and Zylstra, et. al [11]), ignition criteria and theory (Hurricane, et. al [12]) and the historical perspective (Abu-Shawareb, et. al [13]). This design provided more margin for achieving high fusion yields in the presence of perturbations from non-ideal experimental conditions, that reduced performance in the preceding N210808 design which still achieved ignition by Lawson criterion (e.g. large mode one and two asymmetries). Intentional design changes were made to increase the areal density of the DT fuel and capsule at maximum compression which resulted in an increase in performance and fuel burn up fraction.

Prior attempts to increase the DT areal density (ρR) through higher convergence have been unsuccessful in improving the performance and contradictory to expectations from high fidelity plasma physics simulations, likely as a result of increased instabilities that accompany this method of increasing the ρR. Here, we increase the thickness of the diamond capsule that holds the DT fuel to increase the total (DT+capsule) areal density, which is enabled by increasing the laser driver energy on target and adjustments to the implosion symmetry. These changes were proposed directly following N210808, outlined in Kritcher et. al, [9], enabled by improvements to the laser driver efficiency [14, 15].

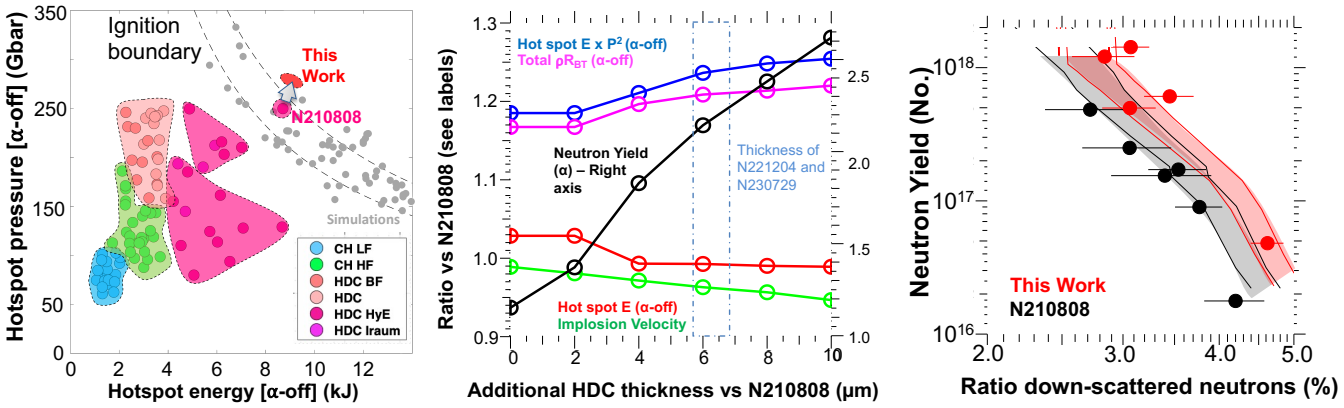

FIG. 2. (left) Increase in ignition metric EP^2: Inferred hot spot pressure (P) and internal energy (E) for previous DT layered experiments at NIF in relation to the ignition boundary (dashed black lines $\sim EP^2$). The grey points under the ignition boundary are from simulations. The increase in ignition metric EP^2 for the N221204 design compared to N210808 is shown in the red shaded region, calculated using a range of assumed perturbations (1D and 3D effects). (middle) Tradeoffs in implosion metrics with increased capsule thickness: Ratio of simulated 1D implosion metrics compared to N210808 as a function of increased HDC (High Density Carbon) ablator thickness. The calculated hot spot E, hot spot EP^2, and total areal density (ρR) are taken at peak compression or "bang time" (peak neutron production) from simulations with α-off. The calculated peak implosion velocities and fusion neutron yields are also shown. (right) Increase in areal density for this work compared to N210808: Neutron yield as a function of DSR, ratio of down scattered neutrons to primary neutrons. Black and red circles are data and the shaded curves are simulations showing the expected increase in DSR at a given yield for this new design from 1D simulations and considering potential 3D degradations, see the text.

EXPERIMENTAL DESIGN

Figure 1 a) shows a schematic of the target and laser configuration. This design uses the indirect-drive approach [16–18] where laser beams are pointed onto the inside of a gold-lined Depleted Uranium (DU) cylindrical can (hohlraum), 11.24 mm length x 6.4 mm diameter, in four distinct laser sets defined by their angle of incidence (Inner beams: 23° & 30° and Outer beams: 44° & 50°). This creates a near black-body radiation oven that is $\sim$ 3 million degrees Kelvin (>300 eV), see Fig. 1 c). The x-rays are absorbed in the outside region of a hollow diamond spherical capsule (ablator) (1050μm inner radius and $\sim$85μm thick) sitting in the center of the hohlraum, which contains the DT fuel (65 μm thick ice layer with a DT gas core). The x-ray absorption heats and ablates the diamond which expands radially outward, causing the remaining diamond capsule and DT fuel to be accelerated inward, or imploded, via the rocket effect at extreme implosion velocities (v_{imp} $\sim$380-400km/s).

A key change in the target configuration for the N221204 design was to thicken the diamond capsule holding the DT fuel by $\sim$5.75μm (N221204) and 6.9μm (N230729) compared to N210808 to provide higher energy coupling of the radiation drive to the hot spot, higher total areal density at peak compression, and improved stability. The amount of % W dopant in the diamond was also increased compared to N210808, see the Appendix. The increase in areal density at maximum compression for the N221204 design vs N210808 can be seen in Fig.1 a) (expanded view) showing the increase in density of the DT shell (top) surrounding the DT hot spot (bottom) from radiation hydrodynamics simulations with the impact of alpha-heating turned off (α-off).

The laser energy was increased from 1.92 to 2.05 MJ at constant peak laser power ($\sim$440TW) by extending the "Peak" of the pulse by 300 ps, see Fig.1 b). The trough of the laser pulse was also extended by 150 ps to maintain the shock timing for the thicker capsule. This resulted in higher and longer duration radiation temperatures compared to N210808, see Fig.1 c). These first experiments were required to increase energy at constant laser power (vs increasing the laser power) as part of the risk mitigation for optics damage in the first stage of enhancing the laser capability. In this work, thicker ablators were used to make optimal use of the extra drive at the end of the pulse which would have otherwise not coupled significantly more driver energy to the implosion. Work is ongoing to further increase the laser power and energy (480TW and 2.2 MJ) which will be used to drive even thicker ($\sim$10-16μm) diamond capsules to high implosion velocities $\sim$400 km/s and low "coasting time"[19], the time between when the radiation drive cools and peak compression.

The longer laser pulse results in more plasma filling into the hohlraum, making it difficult for the "inner" laser beams to propagate to the hohlraum center, creating a reduction in x-ray drive, a more oblate implosion, and reduced energy coupling to the hot spot [20]. The uniformity of the radiation drive was controlled by in-

creasing the amount of laser energy transfer from the "outer" to the "inner" beams, or cross beam energy transfer (CBET), by increasing the detuning of their relative wavelengths ($\Delta\lambda$="Inner" beam - "Outer" beam before laser frequency tripling) [21–24], where $\Delta\lambda$ =1.8$\mathring{A}$ for N210808 and $\Delta\lambda$ =2.75$\mathring{A}$ for N221204. An important advancement for controlling symmetry was the development [23] of CBET in hohlraums with low amounts of He gas fill (0.3 mg/cm^3) [25–27] which achieved high levels of laser light coupling to the hohlraum, ∼96-99%, and low amounts of back-scattered laser light. See the Appendix for a detailed accounting of the laser energy balance into the hohlraum and the implosion.

Fig.1 (a, top) shows radiation hydrodynamics simulations of N221204 (right) compared to N210808 (left) at 6 ns after the start of the laser pulse, with the calculated positions of the material boundaries [gold-lined depleted uranium hohlraum (orange), HDC ablator (light gray), and DT ice layer (blue)] . Overlaid are simulated laser rays showing propagation and absorption within the hohlraum, where the color corresponds to normalized laser powers after CBET. Since the amount of late-time drive symmetry can be difficult to accurately model, a semi-analytical model [28] and measured sensitivity curves [9] were used to determine the optimal $\Delta\lambda$. In addition, precisely adjusting the specific powers on the "inner" and "outer" laser cones during the entire laser pulse (Fig.1 b) enabled controlling fluctuations in the radiation drive uniformity which can induce ρR variations in the compressed fuel and reduce energy coupling. Detailed radiation hydrodynamic simulations using HYDRA [29] with inline CBET [30] were used to design the specific "inner" and "outer" powers. Figure 1 d) shows the calculated increase in power following CBET (e.g. on the 23° cone) and Fig. 1 e) shows the calculated increase in total inner cone power to total power post-CBET together with the input request, see also the Appendix.

These design changes were predicted to increase a key ignition metric EP^2 (by ∼25% compared to N210808), using radiation hydrodynamic simulations, where E is the hot spot internal energy and P is the hot spot pressure at "bang time" from α-off simulations [31], see Fig. 2 (left, red shaded region for this work). Increasing the ignition margin enables igniting the hot spot plasma in the presence of un-intentional perturbations, e.g. low-mode asymmetries [20, 32–35] and radiative loss from ablator mixing into the hot spot [36], and improved robustness for achieving > 1 Megajoule yields. This increase is also expected from analytical theory which predicts EP^2 to increase as the cube of the increased shell mass, assuming symmetry and other implosion parameters could be held constant, giving a 23% increase in EP^2 for an 8% increase in shell mass [12, 37]. The colored points are inferred quantities from prior experiments where the impact of α-heating is removed to better assess proximity to the ignition boundary (dashed black curves)[38]. The grey points under the ignition boundary are from simulations and the red shaded region for this design includes various simulation models to assess the expected increase in EP^2. Experiments to the right of the ignition boundary result in higher burn-up of the DT fuel as the burn-wave post-ignition moves into the cooler denser DT shell.

Figure 2 (middle) shows the tradeoffs in various implosion metrics (1D) that were considered when designing the precise increase in diamond ablator thickness compared to N210808. Following ignition of the hot spot, the simulated fusion energy produced (Neutron Yield α, black curve) increases with increasing total areal density of the fuel and ablator at peak compression (ρR, magenta curve), which provides increased self-heating, hot-spot confinement, and burn-up fraction of the DT fuel [39]. Higher total areal densities can be achieved by driving thicker, higher mass HDC (High Density Carbon) capsules. However, there is a limit on the amount of fuel and capsule mass that can be experimentally driven and still ignite with a fixed driver energy capability and in the presence of non 1-D perturbations. These simulations (1D) reach higher yields than the experiments, and approach the theoretical fuel burn-up fraction. Two dimensional calculations which reproduce the N210808 experimental yield (see Table 1) predict a larger relative increase in performance for the thicker ablator design.

At constant peak laser power, a ∼5.75-6.9μm thicker diamond ablator enabled coupling more of the extended radiation drive to the implosion (∼+ 20 kJ vs N210808) vs extending the drive at constant thickness (∼+ 3 kJ vs N210808). This enabled reaching similar hot spot internal energies (red curve) compared to N210808, even with the reduced fuel implosion velocity (green curve) from the extra target mass at constant laser power. Here, additional PdV work is being done on the hot spot by the imploding remaining ablator material.

One of the goals of this design was to increase the margin for ignition (∼ EP^2) in the presence of known perturbations that reduce the hot spot internal energy or pressure. In choosing a starting thickness, we consider that the hot spot internal energy eventually declines as thickness is increased and the velocity is reduced from the extra mass of the ablator. There exists a theoretical minimum velocity required to ignite the hot spot for a given total areal density [39] which can both be degraded by known issues, low modes and ablator mixing into the hot spot. In addition, thicker ablators are generally more challenging for symmetry due to the longer laser pulse required to maintain shock timing. Therefore, the target thickness increase of ∼5.75-6.9μm was initially chosen to both increase ρR while considering the reduction in implosion velocity and maintaining E. The "coast-time" was also considered as lower implosion velocity leads to later bang times for the same radiation drive, and thus longer coast-times.

Future plans will increase the thickness of the ablator

TABLE I. Simulation metrics for N221204 compared to N210808 and measurements. DSR is defined as the ratio of the escaping 10-12MeV neutrons to the 13-15 MeV neutrons. The subscript $_{BT}$ is taken at time of maximum neutron production and α-off metrics correspond to calculations where the α heating is artificially turned off. Data is listed in parentheses and simulations are listed on the upper cell lines, see the footnote.

"Total degradation" Sims.[1] [Less asym[2], Without low-modes[3]] (Data)	$N210808$	$N221204$
Fusion Yield E_F (MJ)	1.26 [2.25,7.6] (1.37 ±0.04)	3.0 [7.2,13.6] (3.15 ±0.16)
Bang Time (ns)	9.27 [9.28,9.27] (9.28±0.07)	9.61 [9.61,9.58] (9.53±0.07)
DT Ion Temp. (keV)	10.4 [11.6,20] (10.86 ± 0.37)	13.13 [19,27] (13.07 ± 0.74)
Adiabat	2.55-2.75	2.22-2.68
DSR (%)	3.17 [3.0,2.73] (2.72 ± 0.24)	2.93 [2.85,3.08] (2.68 ± 0.16)
Burn-Width (ps)	69 [61,39] (89± 15)	63 [37,33] (70 ± 25)
Implosion Velocity (km/s)	401	383
Remaining Ablator Mass (%)	3.8	5.7
Total ρR_{BT} α-off (g/cm^2)	1.35 [1.38, 1.5]	1.41 [1.5, 1.7]
Total ρR_{BT} (g/cm^2)	1.04 [0.94, 0.87]	0.97 [0.95, 1.12]
HDC ρR_{BT} (g/cm^2)	0.34 [0.31, 0.28]	0.38 [0.35, 0.4]
Fuel ρR_{BT} (g/cm^2)	0.67 [0.60, 0.57]	0.55 [0.55, 0.68]
HS ρR_{BT} (g/cm^2)	0.44 [0.54, 0.56]	0.56 [0.56, 0.65]
Hot Spot Pressure$_{BT}$ (Gbar)	503 [577, 1070]	657 [1315, 1969]
Hot Spot Internal Energy$_{BT}$ (kJ)	85 [147, 374]	181 [332, 533]
Yield Amplification*	29 [50,133]	70 [160,290]
G_{target} (E_F/E_{Laser})	0.65 [1.2,4] (0.71)	1.5 [3.5,6.6] (1.54)

[1] "Total degradation" high-resolution 2D capsule simulations with material roughnesses, a model for the tent and fill tube perturbations, and low mode asymmetries from the hohlraum (Legendre modes: P1, P2, P4).
[2] "Total degradation"[1] 2D simulations with reduced level of P2 flux asymmetry during the "peak" of the drive by 75%.
[3] "Total degradation"[1] 2D simulations without the low mode asymmetries from the hohlraum.
∗Ratio of the yield in simulations where alpha particles deposit energy in the hot spot ("burn on") vs stream freely out of the problem ("burn off"; no-α).

by another 4-10μm to explore the trade-off in ignition margin vs fuel burn-up fraction. Two dimensional "Total degradation" calculations of these designs give > 3 times higher yield compared to this work if symmetry can be maintained and ignition can still be achieved. We also see an increased robustness for the thicker ablator design, or less sensitivity of neutron yield to various degradation mechanisms compared to this current work.

Previously, attempts to increase ρR via higher convergence lower adiabat implosions did not result in higher performance due to enhanced instabilities [40]. As intended, this design increased performance and yield amplification as a result of design changes that increased ρR. The increase in ρR can be observed experimentally by looking at the down scattered ratio (DSR) of primary neutrons in the dense DT surrounding the hot spot with the relationship, $DSR \sim (\rho R_{DT} + \rho R_{HDC}/8)/19$ [31]. Figure. 2 (right) shows the simulated expected increase in DSR at a given neutron yield for the N221204 design (red shaded region) compared to the N210808 (black shaded region). Following maximum compression, the ρR is reduced as the implosion expands and is expected to be lower as yield is increased for a given design. Therefore, it is important to compare ρR improvements at similar fusion yields (see the Appendix Fig. 7).

Since the DSR is weighted more toward the fuel ρR vs the total (fuel + ablator) ρR, the expected increase in DSR at the observed yield level was 7% (see Fig. 7 of the Appendix for the simulated fuel, ablator and total ρR). However, the total (DT + capsule) ρR is a better metric for improved yield amplification than just the fuel ρR, which was calculated to be a larger increase relative to N210808 for this design, ∼20% α-off and ∼15% at higher yields. The shaded region spans the 1D calculated DSR to possible 3D effects, and the filled black circles are experimental data from N210808 and the variability experiments. Achieving a higher DSR at a given yield indicates improvement in the design areal density, which was observed experimentally [11] (black and red points) and by more than the expected amount for the N221204 design compared to the N210808 design [11], and ultimately led to higher burn up fractions of the DT fuel for N221204 (∼4%) compared to N210808 (∼2%). The experimental DSR of N221204 repeat experiments including N230729, the highest gain experiment to date which used a higher quality diamond capsule compared to N221204, are also shown and give the highest measured compression vs yield curve for diamond to date.

Thicker ablators are also better for hydrodynamic stability at the interface between the DT fuel and the diamond ablator which showed a significant reduction in calculated Atwood number for this design compared to N210808, see Fig.8 of the Appendix. This is important for maintaining a higher "clean" (un-mixed) fraction of DT ice as mixing of ablator material into the ice layer can impact compressibility, result in Bremsstrahlung losses,

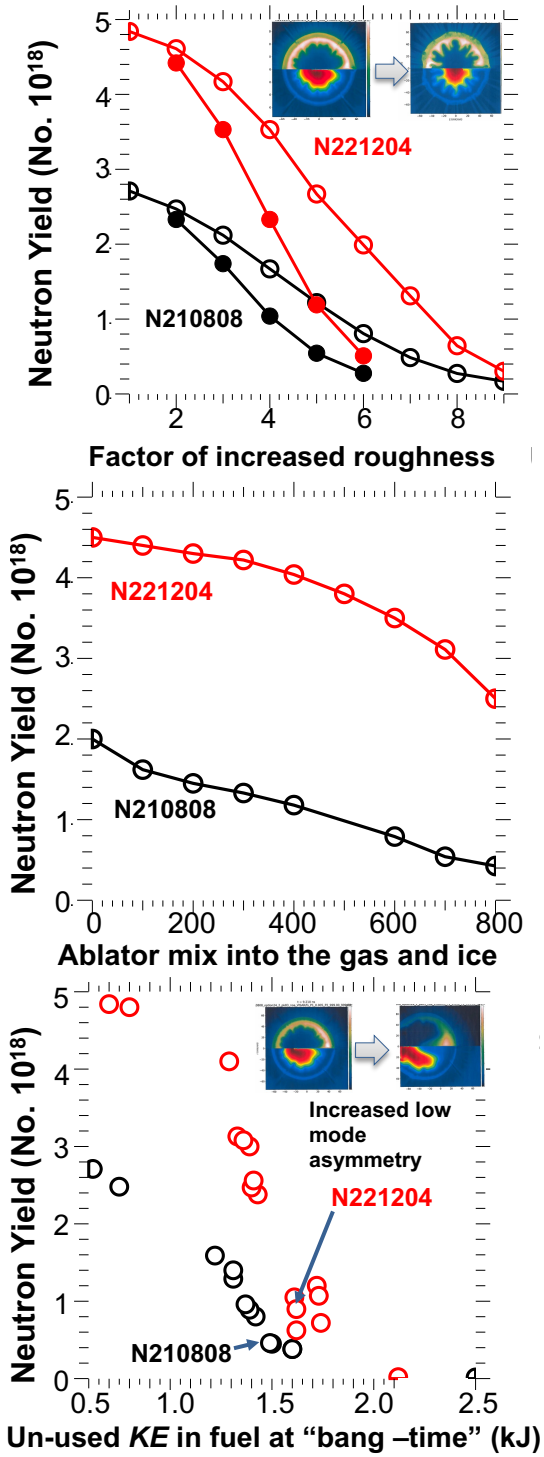

FIG. 3. Increase in simulated performance margin for the N221204 design (red curve and points) compared to the N210808 design (black curve and points) to various perturbations including instabilities from ablator and ice roughness (top, open symbols vary ablator roughness with fixed 1x roughness on the ice, closed symbols vary the ice and ablator roughness), ablator mixing into the hot spot (middle), and low mode asymmetries from the radiation drive (bottom), see the text.

and reduce fuel heating. This reduction of ablator mixing into the ice was observed experimentally for this design confirming the improvement in stability [11].

INCREASED YIELD MARGIN

Figure 3 shows the calculated increase in performance margin (shown in units of neutron yield where $1x10^{18}$ neutrons $\sim$ 2.8MJ of total fusion energy produced) for the N221204 design in this work (red points and curves) compared to the N210808 design (black points and curves) as unintentional perturbations that can reduce the fusion yield are increased. Here, the perturbation magnitude is artificially increased in simulations with larger values along the x-axes. The higher yield margin of the N221204 design enables both producing >1 Megajoule of fusion energy in the presence of enhanced perturbations compared to N210808, as well as higher yields if the same low level of perturbations as observed on N210808 can be achieved. The types of perturbations shown in Fig. 3 are main sources of yield degradation in nearly all of the ignition experiments and are difficult to control so, therefore, increasing margin to these perturbations is important.

Figure 3 (top) shows higher 2D simulated neutron yield for N221204 vs N210808 as a function of increased surface roughness (as factors of the nominal values) on the tungsten doped and un-doped diamond ablator interfaces and 1.0x roughness on the ice (open symbols) as well as roughness applied to the doped and un-doped interfaces as well as the ice layer as denoted by the x-axis (closed symbols). These simulations model the tent perturbation feature, DT fill-tube perturbation feature, and surface roughnesses ("Total degradation"[1] 2D simulations without the low mode asymmetries from the hohlraum in Table 1). This perturbation can arise from worse target and ice-layer quality and also act as a surrogate in simulations for increased interface instability. Example simulated images from α-off simulations are shown as insets for the nominal case and an increased roughness case. The top half of the inset shows the density contour at peak compression and the bottom half shows the ion temperature at peak compression.

Figure 3 (middle) shows higher neutron yield for the N221204 design vs the N210808 design to a given level of ablator mixing into the inner 10μm of DT ice and volumetrically into the hot spot (mass in ng), which can radiate energy away and cools the hot spot. Here, the calculations use Non-local thermodynamic equilibrium (Non-LTE) atomic physics tables in 1D to accurately model the radiative losses. This mixing can be seeded by isolated defects in the diamond ablator such as pits on the outer diamond surface, voids in the diamond shell, engineering features, and hohlraum material that can flake onto the capsule. In this design, increasing the amount of energy coupled to the hot spot enables tolerating higher levels

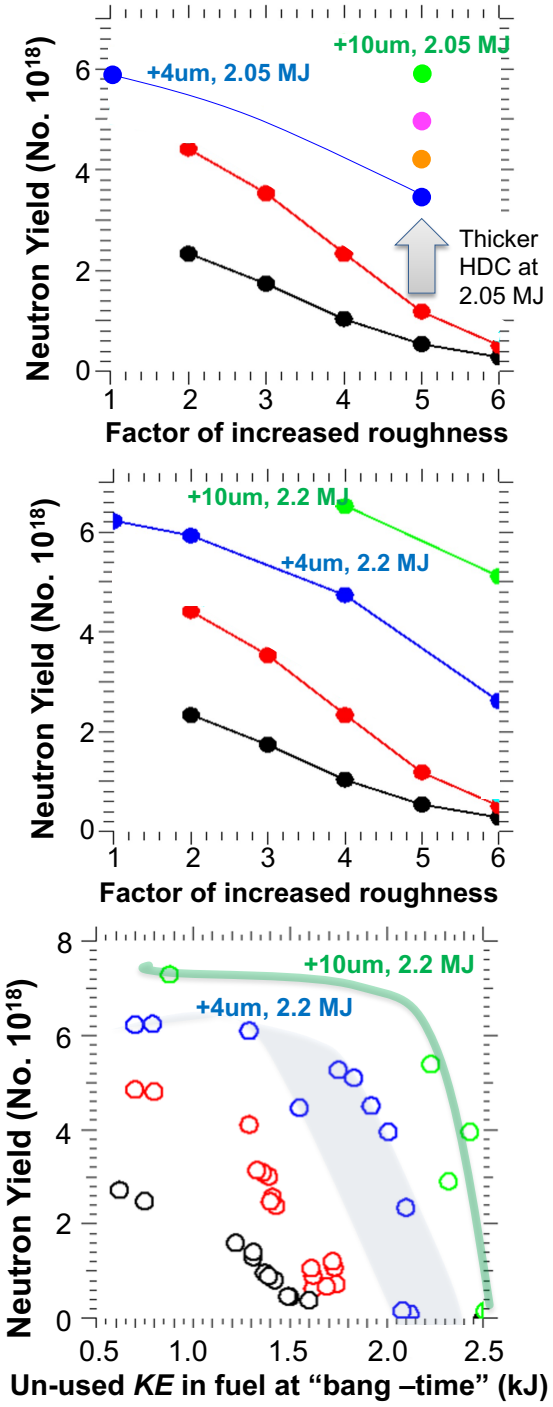

FIG. 4. (top) Simulated increase yield as a function of increased roughness of the diamond ablator interfaces and ice layer for future designs that further increase the diamond ablator thickness compared to N221204 (red curve) by an additional 4 μm (blue points), 6 μm (orange), 8 μm (magenta), and 10 μm (green) using the same 2.05 MJ laser energy and hohlraum geometry with adjusted shock timing. Increase in simulated performance as a function of increased roughness (middle) of the diamond and ice layers and increased low mode asymmetries from the radiation drive (bottom) for further increasing the diamond ablator thickness compared to N221204 (red curve) by an additional 4 μm (blue points) and 10 μm (green) using 2.2 MJ of laser energy and hohlraum geometry with adjusted shock timing. The black points and curves are simulations of the N210808 design.

of these isolated capsule defects.

Higher simulated performance for the N221204 vs N210808 design as a function of increased low mode asymmetries is shown in Fig. 3 (bottom), using "Total degradation"[1] 2D simulations (see Table 1) with varying amounts of applied modes P1, P2, & P4, Legendre moments of the radiation flux asymmetry. Here, the x-axis is the amount of left over work that was not done on the hot spot, or residual kinetic energy (RKE) from α-off simulations, as a result of the low mode asymmetries creating an inefficient piston. As a result the N221204 design can tolerate higher levels of this perturbation and still achieve high performance compared to N210808. These low mode asymmetries are another leading source of degredation for ignition experiments, which can be seeded by non-uniformities in the capsule and ice thicknesses as well as imbalances in the laser power delivery. Simulations estimate that the low mode asymmetries still resulted in a 4.5x yield reduction for N221204, compared to a 32% yield reduction from roughness on the diamond and ice interfaces. Work is ongoing to improve these asymmetries for higher performance.

In addition to improving these perturbations, ongoing work aims to further increase the performance margin and robustness, or insensitivity, to these perturbations. This can be seen in Fig.4 which shows that the yield can be substantially increased for a given level of increased roughness of the ablator and ice interfaces by further increasing the diamond thickness of the N221204 design using the same hohlraum configuration, laser energy, and adjusted shock timing. These changes are expected to increase total areal density and energy coupled to the implosion. The tradeoff of this design change is reduced velocity due to the extra ablator payload and risk for achieving symmetry due to the longer pulse (adjusted shock timing) and extra ablator payload.

The first tests of the thicker ablator higher energy design (this work) managed these risks by taking a substantial but smaller first step. Future experiments will continue to pursue thicker ablators using 2.05 MJ of laser energy. In addition the robustness and yield margin can be further increased with the thicker ablators using an extended 2.2 MJ laser driver, see Fig.4 (middle: yield vs roughness factor and bottom: yield vs low mode asymmetry). For the 2.2 MJ design with a 10μm thicker diamond ablator compared to N221204 (green curves) the yield vs perturbation becomes less sensitive, i.e. more robust. We predict that these designs meet the threshold for minimum velocity to ignite the hot spot and would further increase the total areal density for higher fuel burn-up fraction. Additional design modifications are predicted to improve performance by $> 2x$ and will be tested sequentially, including increasing the laser power of the 2.05 and 2.2 MJ designs up to 500TW to increase the coupling and implosion velocity, reducing the central gas fill in the capsule for higher convergence, and

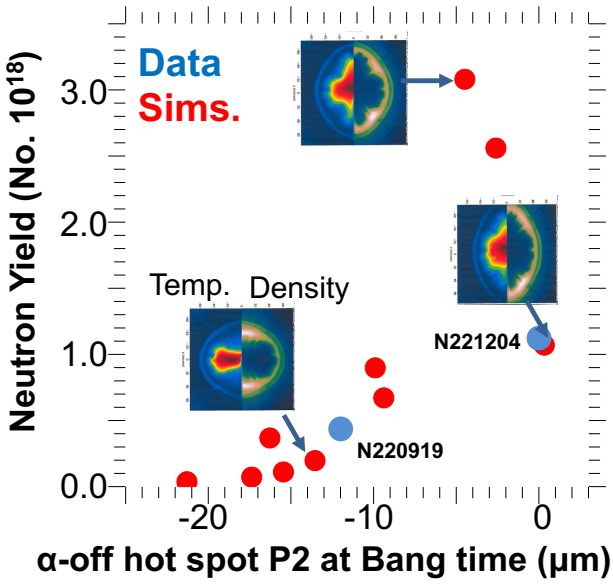

FIG. 5. Simulated sensitivity of α-on fusion energy yield to hot spot oblateness (-P2) from α-off simulations, using a "Total degradation" model of the N221204 design (red points), where the flux asymmetry was adjusted in the simulations to vary hot spot P2. The hot spot P2 was ~-12μm for N220919 and ~0μm for N221204. We predicted that a performance increase of >2 x vs N220919 could be achieved by improving the hot spot P2 to within a few μm of round, and a higher increase in performance if the hot spot was closer to round (P_2=0). The range of yields at a given level of hot spot P2 results from different assumptions about the magnitude of the time-varying P2 of the hot spot and DT shell, which will be benchmarked against data in coming experiments.

increasing the DT fuel mass.

The extra margin in performance of the N221204 design, compared to N210808, to low mode asymmetries was demonstrated on the first test of the new thicker ablator higher energy design on Sept. 19, 2022 (N220919) which had a significant level of P2 asymmetry in the hot spot plasma (P2 $\sim -12\mu m$), reducing energy coupling to the hot spot. However, due to the increase in performance margin, this experiment still produced high fusion energy ~1.22 MJ, and was the second experiment on NIF to reach > 1 MJ. We estimate that this level of asymmetry would have reduced the yield to < 1×10^{17} neutrons (< 280 kJ) in the N210808 design. Changes made to improve only this asymmetry between N220919 and N221204 resulted in >2.5 times increase in fusion energy yield (3.15 MJ) and the first controlled fusion experiment to ever reach target gain greater than unity (~1.5). The symmetry changes include increasing the amount of wavelength separation from $\Delta\lambda = 2.5\AA$ to $\Delta\lambda = 2.75\AA$ and optimizing the time-dependent radiation drive symmetry based on an updated model tuned to data which was acquired in 2022, see the Appendix for more details.

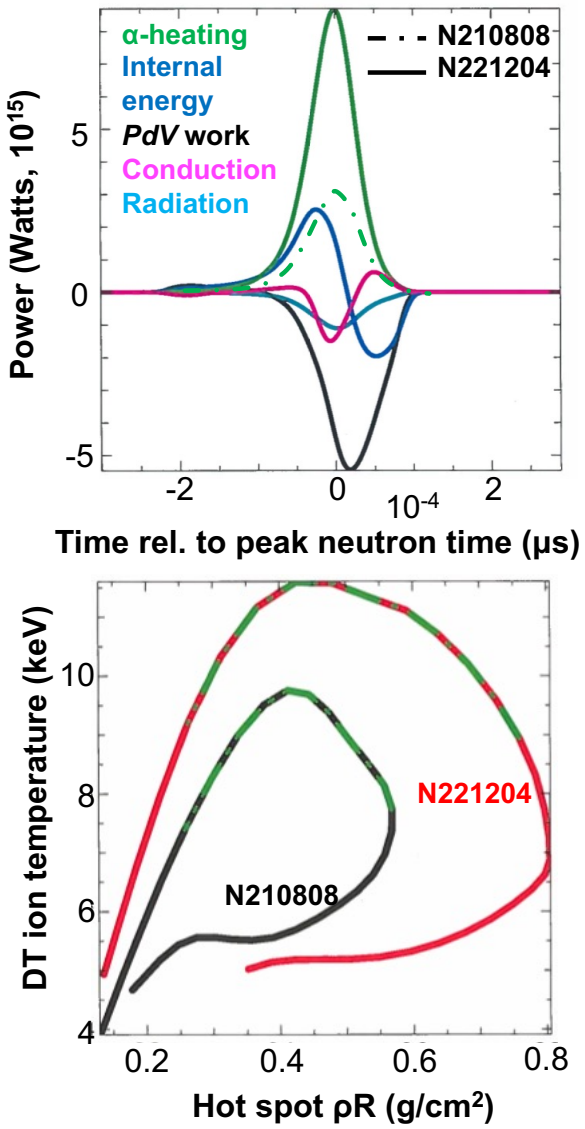

FIG. 6. (top) Temporal histories of the simulated hot spot power (Watts) balance for N221204 (dashed curves) compared to N210808 (solid curves), normalized to the respective "bang-times" (peak neutron production) showing significantly higher α-heating for N221204. (bottom) Simulated hot spot areal density vs ion temperature for N221204 (red curve) vs N210808 (black curve) showing higher initial areal densities for N221204 and a substantial increase in areal density and ion temperature over the burn duration. Here, "bang time" $\pm$ 50 ps is denoted by the green dashed curves.

The expected increase in yield as a result of fixing the symmetry was accurately predicted using a HYDRA "Total degradation" model calibrated to N220919, see Fig. 5. Here, the red points are simulations of the dependence of the neutron yield on the level of hot spot oblateness (P2) for the N221204 thicker ablator higher energy design. The level of oblateness is calculated by taking the Legendre decomposition of the 17% peak neutron or x-

ray emission contour. The range of simulated neutron yields at a given level of hot spot oblateness is due to uncertainty in the calculated time history of fluctuations in hot spot and dense DT fuel asymmetry. The insets are simulated contours at peak compression from α-off simulations of the the hot spot temperature (left) and dense DT fuel shape (right) for example points. The measured level of hot spot oblateness for N220919 vs N221204 (blue points) follows the simulation curve which predicted that fixing the symmetry would result in target gain > 1 and achievement of ignition at the NIF by all metrics including the NAS definition.

A mode one asymmetry also varied between these experiments, with a measured hot spot velocity of 36 km/s for N221204 compared to 67 km/s for N210808. Since the sensitivity of neutron yield to mode one asymmetry is design dependent, and depends on the presence of other sources of yield degradation, it is important to estimate the impact of mode one in simulations that include the other known sources of degradations (P2, P4 tent, fill tube, roughness) and also match the experimental neutron yield.

From simulations, we estimate that the measured mode one reduced the yield by $\sim$25% for N210808 and by $<$10% for N221204, and that the difference in neutron yield between these experiments as a result of mode one was $\sim$10%. However, the neutron yield increased by $>$ 2.5x with the P2 asymmetry correction which was the dominant source of improved symmetry. In addition, a repeat experiment of N221204 (N230729) displayed a higher observed mode one asymmetry of $\sim$104 km/s (also simulated to reduce the neutron yield by $\sim$25%) but still achieved the highest yield to date of 3.88 MJ and $>$2.8x higher neutron yield than N210808. The experimental sources for the observed mode one asymmetries in these experiments will be outlined in a future publication.

We also used a Cognitive-Simulation Machine Learning (ML) model to generate a probability distribution for achieving target gain > 1 given these design parameters and previously observed levels of degradations, which predicted a 50% chance for this new design to achieve target gain > 1 compared to 17% for N210808 [41].

SIMULATED HOT SPOT CONDITIONS

Figure 6 shows these design changes resulted in a substantial increase in calculated alpha heating power (in Watts) for N221204 (solid lines) compared to N210808 (dashed line). The amount of simulated self-heating power from the alpha particles is $\sim$ three times higher for N221204 which burned up $\sim$ 2.3 times more DT fuel. The difference in simulated increase in the alpha heating power compared to the burn up fraction for these experiments is due to differences in the burn duration and in the magnitude of the power loss mechanisms.

This analysis uses detailed radiation hydrodynamic (HYDRA) post-shot "Total degradation" simulations that match the experimental hot-spot observables, see Table I. Here the time axis is shifted relative to the time of peak neutron production. The α-particle heating for N221204 (green curve) is greater than the initial PdV work done on the hot spot (black curve) as well as the energy loss mechanisms (conduction and radiative loss), and for a long enough duration of time (confinement time), which enables the plasma to "ignite" and a thermodynamic instability in DT plasma self-heating occurs. The alpha heating power is so high that the internal energy (blue curves) continues to rise even in the presence of losses including energy loss resulting from the explosion phase when the PdV work becomes negative and removes energy from the hotspot.

The increase in calculated alpha heating power is largely due to the increase in calculated hot spot areal density for N221204 vs N210808. This increase can be seen in Fig. 6 (bottom) which shows the evolution in time of the hot spot ρR vs ion temperature for N221204 (red curve) vs N210808 (black curve). The overlaid green dashed curves denote "bang-time" $\pm 50ps$. Here, N221204 starts out at similar hot spot temperature but higher hot spot areal density, which leads to an increase in alpha heating and then a substantial increase in hot spot ρR and temperature. The reversal of the trajectory to lower areal densities throughout the burn for both experiments is due to the hot spot continuing to increase in temperature on expansion.

CONCLUSION

In summary, the design changes presented in this paper resulted in the first ever controlled fusion experiment (N221204) to exceed target gain greater than unity, where the fusion energy produced exceeded the energy used to drive the target by $\sim$1.9x. This design used a thicker diamond capsule (additional $\sim$ 7.6% in thickness) together with an extended higher energy laser drive (additional $\sim$ 7% in energy)[14, 15] to increase the margin for ignition and enable higher DT fuel burn up fractions compared to N210808 ($\sim$4.3% compared to $\sim$1.9%). This proof-of-principle experiment demonstrates that there is nothing fundamentally limiting fusion energy gain in the laboratory. Since this manuscript was drafted, a repeat experiment with a higher quality diamond ablator (fewer high-Z inclusions) resulted in a new record yield of $\sim$3.88MJ and fusion energy target gain of $\sim$1.9. Small adjustments to the laser input conditions were also made for the new capsule.

This work builds on the previous HYBRID-E design N210808 and further increases the α-off total areal density by $\sim$20% which led to a DSR increase at a given yield of $>$14% which was higher than predicted. The

first test of this new design (N220919) showed an intrinsic P2 asymmetry from the hohlraum radiation drive but still produced ∼1.2 MJ fusion energy. Changes only to optimize the implosion symmetry for N221204 resulted in a >2.5 times increase in fusion energy as predicted by high fidelity radiation hydrodynamic simulations and theoretical models. This platform will be the basis for future designs including an effort to extend the laser drive to 2.2 MJ and increase the HDC ablator thickness by an additional ∼10μm.

This work was performed under the auspices of U.S. Department of Energy by Lawrence Livermore National Laboratory under Contract DE-AC52-07NA27344. This document was prepared as an account of work sponsored by an agency of the United States government. Neither the United States government nor Lawrence Livermore National Security, LLC, nor any of their employees makes any warranty, expressed or implied, or assumes any legal liability or responsibility for the accuracy, completeness, or usefulness of any information, apparatus, product, or process disclosed, or represents that its use would not infringe privately owned rights. Reference herein to any specific commercial product, process, or service by trade name, trademark, manufacturer, or otherwise does not necessarily constitute or imply its endorsement, recommendation, or favoring by the United States government or Lawrence Livermore National Security, LLC. The views and opinions of authors expressed herein do not necessarily state or reflect those of the United States government or Lawrence Livermore National Security, LLC, and shall not be used for advertising or product endorsement purposes.

* kritcher2@llnl.gov

[1] E. I. Moses *et al.*, The national ignition facility: Transition to a user facility, Journal of Physics: Conference Series **688**, 012073 (2016).

[2] S. E. Koonin, G. F. Carrier, R. Christy, R. Conn, R. Davidson, J. Dawson, A. DeMaria, P. Doty, W. Happer Jr., G. L. Kulcinski, *et al.*, Review of the department of energy's inertial confinement fusion program, Journal of Fusion Energy **10**, 157 (1991).

[3] J. Nuckolls, L. Wood, A. Thiessen, and G. Zimmerman, Laser compression of matter to super-high densities: Thermonuclear (ctr) applications, Nature **239**, 139 (1972).

[4] J. S. Clarke, H. N. Fisher, and R. J. Mason, Laser-driven implosion of spherical dt targets to thermonuclear burn conditions., Phys. Rev. Lett. **30**, 249 (1973).

[5] R. F. Post, Controlled fusion research—an application of the physics of high temperature plasmas, Rev. Mod. Phys. **28**, 338 (1956).

[6] G. S. Fraley, E. J. Linnebur, R. J. Mason, and R. L. Morse, The Physics of Fluids **17**, 474 (1974).

[7] J. D. Lawson, Some criteria for a power producing thermonuclear reactor, Proceedings of the Physical Society. Section B **70**, 6 (1957).

[8] H. Abu-Shawareb, (Indirect Drive ICF Collaboration), *et al.*, Lawson's criterion for ignition achieved in an inertial fusion experiment, Phys. Rev. Lett. **129** (2022).

[9] A. L. Kritcher, A. L. Kritcher, A. B. Zylstra, D. A. Callahan, O. A. Hurricane, C. R. Weber, D. S. Clark, C. V. Young, J. E. Ralph, D. T. Casey, A. Pak, O. L. Landen, *et al.*, Phys. Rev. E **106** (2022).

[10] A. Zylstra *et al.*, Phys. Rev. E **106** (2022).

[11] A. Pak, A. Zylstra, K. L. Baker, D. T. Casey, E. Dewald, L. Divol, M. Hohenberger, A. S. Moore, J. E. Ralph, D. J. Schlossberg, *et al.*, Observations and properties of the first laboratory fusion experiment to exceed target gain of 1, Phys. Rev. E **Submitted** (2023).

[12] O. A. Hurricane, D. A. Callahan, D. T. Casey, A. R. Christopherson, A. L. Kritcher, O. L. Landen, S. A. Maclaren, R. Nora, P. Patel, J. Ralph, D. Schlossberg, P. T. Springer, C. V. Young, and A. B. Zylstra, Energy principles of scientific breakeven in an inertial fusion experiment, Phys. Rev. L **Submitted** (2023).

[13] I. D. I. C. Abu-Shawareb, H. *et al.*, Achievement of target gain larger than unity in an inertial fusion experiment, Phys. Rev. Lett. (2023).

[14] J.-M. Di Nicola, T. Suratwala, L. Pelz, J. Heebner, D. Alessi, A. Bhasker, T. Bond, M. Bowers, G. Brunton, B. Buckley, *et al.*, Proc. SPIE PC12401, High Power Lasers for Fusion Research VII , PC1240103 (2023).

[15] J. D. Nicola, T. Bond, M. Bowers, L. Chang, M. Hermann, R. House, T. Lewis, K. Manes, G. Mennerat, B. MacGowan, R. Negres, B. Olejniczak, C. Orth, T. Parham, S. Rana, B. Raymond, M. Rever, S. Schrauth, M. Shaw, M. Spaeth, B. V. Wonterghem, W. Williams, C. Widmayer, S. Yang, P. Whitman, and P. Wegner, The national ignition facility: laser performance status and performance quad results at elevated energy, Nuclear Fusion **59**, 032004 (2018).

[16] J. Lindl, Development of the indirect-drive approach to inertial confinement fusion and the target physics basis for ignition and gain, Phys. Plasmas **2**, 3933 (1995).

[17] J. D. Lindl, P. Amendt, R. L. Berger, S. G. Glendinning, S. H. Glenzer, S. W. Haan, R. L. Kauffman, O. L. Landen, and L. J. Suter, The physics basis for ignition using indirect-drive targets on the national ignition facility, Phys. Plasmas **11**, 339 (2004).

[18] S. W. Haan, J. D. Lindl, D. A. Callahan, D. S. Clark, J. D. Salmonson, B. A. Hammel, L. J. Atherton, R. C. Cook, M. J. Edwards, S. H. Glenzer, *et al.*, Point design targets, specifications, and requirements for the 2010 ignition campaign on the National Ignition Facility, Phys. Plasmas **18**, 051001 (2011).

[19] O. A. Hurricane, A. Kritcher, D. A. Callahan, O. Landen, P. K. Patel, P. T. Springer, D. T. Casey, E. L. Dewald, T. R. Dittrich, T. Döppner, *et al.*, On the importance of minimizing "coast-time" in x-ray driven inertially confined fusion implosions, Phys. Plasmas **24**, 092706 (2017).

[20] A. L. Kritcher, R. Town, D. Bradley, D. Clark, B. Spears, O. Jones, S. Haan, P. T. Springer, J. Lindl, R. H. H. Scott, *et al.*, Metrics for long wavelength asymmetries in inertial confinement fusion implosions on the National Ignition Facility, Phys. Plasmas **21**, 042708 (2014).

[21] P. Michel, L. Divol, E. A. Williams, S. Weber, C. A. Thomas, D. A. Callahan, S. W. Haan, J. D. Salmonson, S. Dixit, D. E. Hinkel, *et al.*, Tuning the implosion symmetry of icf targets via controlled crossed-beam energy

transfer, Phys. Rev. Lett. **102**, 025004 (2009).
[22] J. D. Moody, P. Michel, L. Divol, R. L. Berger, E. Bond, D. K. Bradley, D. A. Callahan, E. L. Dewald, S. Dixit, M. J. Edwards, *et al.*, Multistep redirection by cross-beam power transfer of ultrahigh-power lasers in a plasma, Nature Physics **8**, 344 (2012).
[23] A. L. Kritcher, J. Ralph, D. E. Hinkel, T. Döppner, M. Millot, D. Mariscal, R. Benedetti, D. J. Strozzi, T. Chapman, Goyon, *et al.*, Energy transfer between lasers in low-gas-fill-density hohlraums, Phys. Rev. E **98**, 053206 (2018).
[24] L. A. Pickworth, T. Doeppner, D. E. Hinkel, J. E. Ralph, B. Bachmann, L. P. Masse, L. Divol, L. R. Benedetti, P. M. Celliers, H. Chen, *et al.*, Phys. Plasmas **27**, 102702 (2020).
[25] S. L. Pape, L. F. B. Hopkins, L. Divol, N. Meezan, D. Turnbull, A. J. Mackinnon, D. Ho, J. S. Ross, S. Khan, A. Pak, *et al.*, The near vacuum hohlraum campaign at the NIF: A new approach, Phys. Plasmas **23**, 056311 (2016).
[26] L. F. Berzak Hopkins, N. B. Meezan, S. Le Pape, L. Divol, A. J. Mackinnon, D. D. Ho, M. Hohenberger, O. S. Jones, G. Kyrala, J. L. Milovich, *et al.*, First high-convergence cryogenic implosion in a near-vacuum hohlraum, Phys. Rev. Lett. **114**, 175001 (2015).
[27] L. Divol, A. Pak, L. F. B. Hopkins, S. L. Pape, N. B. Meezan, E. L. Dewald, D. D.-M. Ho, S. F. Khan, A. J. Mackinnon, J. S. Ross, *et al.*, Symmetry control of an indirectly driven high-density-carbon implosion at high convergence and high velocity, Phys. Plasmas **24**, 056309 (2017).
[28] D. A. Callahan, O. A. Hurricane, J. E. Ralph, C. A. Thomas, K. L. Baker, L. R. Benedetti, L. F. Berzak Hopkins, D. T. Casey, T. Chapman, C. E. Czajka, *et al.*, Exploring the limits of case-to-capsule ratio, pulse length, and picket energy for symmetric hohlraum drive on the National Ignition Facility Laser, Phys. Plasmas **25**, 5 (2018).
[29] M. M. Marinak, G. D. Kerbel, N. A. Gentile, O. Jones, D. Munro, S. Pollaine, T. R. Dittrich, and S. W. Haan, Three-dimensional hydra simulations of national ignition facility targets, Phys. Plasmas **8**, 2275 (2001).
[30] D. J. Strozzi, D. S. Bailey, P. Michel, L. Divol, S. M. Sepke, G. D. Kerbel, C. A. Thomas, J. E. Ralph, J. D. Moody, and M. B. Schneider, Interplay of laser-plasma interactions and inertial fusion hydrodynamics, Phys. Rev. Lett. **118**, 025002 (2017).
[31] J. D. Lindl, S. W. Haan, O. L. Landen, A. R. Christopherson, and R. Betti, Progress toward a self-consistent set of 1d ignition capsule metrics in icf, Phys. Plasmas **25**, 122704 (2018).
[32] D. Casey *et al.*, Casey,d. and macgowan, b. and hurricane,o. and landen, o. and nora, r. and haan, s. and kritcher, a. and zylstra, a. and ralph, j. and dewald, e. and others, Phys. Rev. E **108** (2023).
[33] O. A. Hurricane, D. T. Casey, O. Landen, A. L. Kritcher, R. Nora, P. K. Patel, J. A. Gaffney, K. D. Humbird, J. E. Field, M. K. G. Kruse, J. L. Peterson, and B. K. Spears, An analytic asymmetric-piston model for the impact of mode-1 shell asymmetry on icf implosions, Phys. Plasmas **27**, 062704 (2020).
[34] B. MacGowan, O. Landen, D. Casey, C. Young, D. Callahan, E. Hartouni, R. Hatarik, M. Hohenberger, T. Ma, D. Mariscal, *et al.*, Trending low mode asymmetries in NIF capsule drive using a simple viewfactor metric, High Energy Density Physics **40**, 100944 (2021).
[35] D. T. Casey, B. J. MacGowan, J. D. Sater, A. B. Zylstra, O. L. Landen, J. Milovich, O. A. Hurricane, A. L. Kritcher, M. Hohenberger, K. Baker, *et al.*, Evidence of three-dimensional asymmetries seeded by high-density carbon-ablator nonuniformity in experiments at the national ignition facility, Phys. Rev. Lett. **126**, 025002 (2021).
[36] A. Pak, L. Divol, C. R. Weber, L. F. B. Hopkins, D. S. Clark, E. L. Dewald, D. N. Fittinghoff, V. Geppert-Kleinrath, M. Hohenberger, S. Le Pape, *et al.*, Impact of localized radiative loss on inertial confinement fusion implosions, Phys. Rev. Lett. **124**, 145001 (2020).
[37] O. A. Hurricane, D. T. Casey, O. Landen, D. A. Callahan, R. Bionta, S. Haan, A. Kritcher, R. Nora, P. Patel, P. Springer, *et al.*, Phys. Plasmas **29**, 012703 (2022).
[38] P. K. Patel, P. T. Springer, C. R. Weber, L. C. Jarrott, O. A. Hurricane, B. Bachmann, K. L. Baker, L. F. B. Hopkins, D. A. Callahan, D. Casey, *et al.*, Hotspot conditions achieved in inertial confinement fusion experiments on the national ignition facility, Phys. Plasmas **27**, 050901 (2020).
[39] J. Lindl, S. Haan, and O. L. Landen, Impact of hohlraum cooling on ignition metrics for inertial fusion implosions, Phys. Plasmas **30** (2023).
[40] O. A. Hurricane, D. A. Callahan, P. T. Springer, M. J. Edwards, P. Patel, K. Baker, D. T. Casey, L. Divol, T. Doeppner, D. E. Hinkel, *et al.*, Beyond alpha-heating: driving inertially confined fusion implosions toward a burning-plasma state on the national ignition facility, Plasma Phys. Control. Fusion **61**, 014033 (2019).
[41] B. K. Spears, S. Brandon, J. E. Field, J. Gaffney, K. D. Humbird, K. A. L., M. K. G. Kruse, E. Kur, B. Kustowski, D. Munro, *et al.*, A physics-informed machine learning model quantitively predicted fusion ignition at the national ignition facility, Science **in progress** (2023).
[42] D. S. Clark, C. Weber, *et al.*, Three-dimensional simulations of low foot and high foot implosion experiments on the National Ignition Facility, Phys. Plasmas **23** (2016), 57th Annual Meeting of the APS-Division-of-Plasma-Physics (DPP), Savannath, GA, NOV 16-20, 2015.
[43] D. S. Clark, C. R. Weber, J. L. Milovich, A. E. Pak, D. T. Casey, B. A. Hammel, D. D. Ho, O. S. Jones, J. M. Koning, A. L. Kritcher, *et al.*, Three-dimensional modeling and hydrodynamic scaling of national ignition facility implosions, Phys. Plasmas **26**, 050601 (2019).
[44] L. X. L. Benedict, K. P. Driver, S. Hamel, B. Militzer, T.Qi, A. A. Correa, A. Saul, and E. Schwegler, Multiphase equation of state for carbon addressing high pressures and temperatures, Phys. Rev. B **89**, 224109 (2014).
[45] J. Gaffney, S. Hu, P. Arnault, A. Becker, L. Benedict, T. Boehly, P. Celliers, D. Ceperley, O. Certik, J. Clerouin, *et al.*, A review of equation-of-state models for inertial confinement fusion materials, High Energy Density Physics **28**, 7 (2018).
[46] M. P. Desjarlais, C. R. Scullard, L. X. Benedict, H. D. Whitley, and R. Redmer, Density-functional calculations of transport properties in the nondegenerate limit and the role of electron-electron scattering, Phys. Rev. E **95**, 033203 (2017).
[47] L. G. Stanton and M. S. Murillo, Ionic transport in high-energy-density matter, Phys. Rev. E **93**, 043203 (2016).
[48] C. A. Iglesias and F. J. Rogers, Updated Opal Opacities,

Astrophys. J. **464**, 943 (1996).
[49] Y. Lee and R. More, An electron conductivity model for dense plasmas, The Physics of Fluids **27**, 1273 (1984).
[50] C. R. Scullard, S. Serna, L. X. Benedict, C. L. Ellison, and F. R. Graziani, Analytic expressions for electron-ion temperature equilibration rates from the lenard-balescu equation, Phys. Rev. E **97**, 013205 (2018).
[51] A. Correa, L. Benedict, D. Young, E. Schwegler, and S. A. Bonev, Phys. Rev. B **78** (2008).
[52] N. B. Meezan, D. T. Woods, N. Izumi, H. Chen, H. A. Scott, M. B. Schneider, D. A. Liedahl, O. S. Jones, G. B. Zimmerman, J. D. Moody, O. L. Landen, and W. W. Hsing, Evidence of restricted heat transport in national ignition facility hohlraums, Phys. Plasmas **27**, 102704 (2020).
[53] R. Kirkwood, D. Strozzi, P. Michel, D. Callahan, B. Raymond, G. Gururangan, B. MacGowan, N. Team, *et al.*, Laser backscatter damage risk assessments of NIF target experiments, in *APS Meeting Abstracts* (2014).
[54] A. Kritcher, C. Young, H. Robey, C. Weber, A. Zylstra, O. Hurricane, D. Callahan, J. Ralph, J. Ross, K. Baker, *et al.*, Design of implosions reaching the burning plasma regime, Nature Physics **18**, 251 (2022).
[55] A. L. Kritcher, D. T. Casey, C. A. Thomas, A. Zylstra, M. Hohenberger, K. Baker, S. Le Pape, B. Bachmann, S. Bhandarkar, J. Biener, *et al.*, Phys. Plasmas **27**, 052710 (2020).
[56] A. L. Kritcher, A. B. Zylstra, D. A. Callahan, O. A. Hurricane, C. Weber, J. Ralph, D. T. Casey, A. Pak, K. Baker, B. Bachmann, *et al.*, Achieving record hot spot energies with large hdc implosions on NIF in Hybrid-E, Phys. Plasmas **28**, 072706 (2021).

APPENDIX

Simulation Methodology

The simulations were performed using a radiation hydrodynamics plasma physics code HYDRA [29] to model the radiation drive created by the laser-hohlraum interaction and the physics of the capsule implosion. These simulations were performed in a two step process; First, integrated simulations of the hohlraum and capsule implosion that are benchmarked against experimental data from focused tuning experiments, are used to determine the spatially, temporally, and frequency resolved radiation drive surrounding the capsule implosion. Then, the radiation drive is extracted and applied to higher resolution capsule-only "Total degradation" simulations of the implosion to model engineering features with higher fidelity, such as material roughness of the capsule interfaces, a model for the capsule support tent, a model for the DT fill tube [42, 43], non-uniformities in ablator thickness and DT fuel layer thickness together with low mode non-uniformities of the radiation drive (including mode one, two, and four). The radiation hydrodynamic calculations include detailed equations of state [44, 45], radiation particle and neutron transport models [46, 47], opacity models[48]), and electron-ion coupling [49, 50]. In this study, the equation of state model used for the carbon ablator was LEOS table 9067 [51]. The radiation drive is modeled with a flux-limited electron heat transport with a limiter of 0.15 which has been shown to reproduce many radiation drive observables for similar hohlraum conditions [52]. An in-line cross beam energy transfer model was used with a saturation clamp on the electron density fluctuations of the ion acoustic wave ($\delta n/n$). Post-shot simulations (after the experiment) use the measured input target conditions and as-delivered laser powers vs time for all beams which can vary from the requested input conditions.

The simulations are adjusted in a common way between experiments to match tuning data and then applied to simulate the DT layered experiments. These adjustments include artificial multipliers on the input laser power to the integrated simulations to match the in-flight symmetry, in-flight capsule velocity, and shock velocities along two lines of sight (pole and equator). Recent shock timing data prior to N221204 was obtained which improved the symmetry model for temporal variations in the radiation drive when applied to this new design. This data together with the in-flight symmetry and DT hot spot symmetry set the saturation clamp $\delta n/n = 0.002$ in the "foot" of the laser pulse until the beginning of the rise to peak power and $\delta n/n$=0.0075 throughout the remainder of the laser pulse. Back-scattered laser light due to interaction of the lasers with the hohlraum wall plasma was energetically small on (210808, 221204). This is mostly due to Stimulated Brillouin Scattering (SBS) [53] of the inner beams early in peak laser power. The simulations reported here do not model this explicitly, but as part of an effective total laser power multiplier and $\delta n/n$. Recent work suggests that including the measured backscatter time history could impact implosion shape.

For additional details on the simulation methodology see, ref. [9, 23, 54, 55].

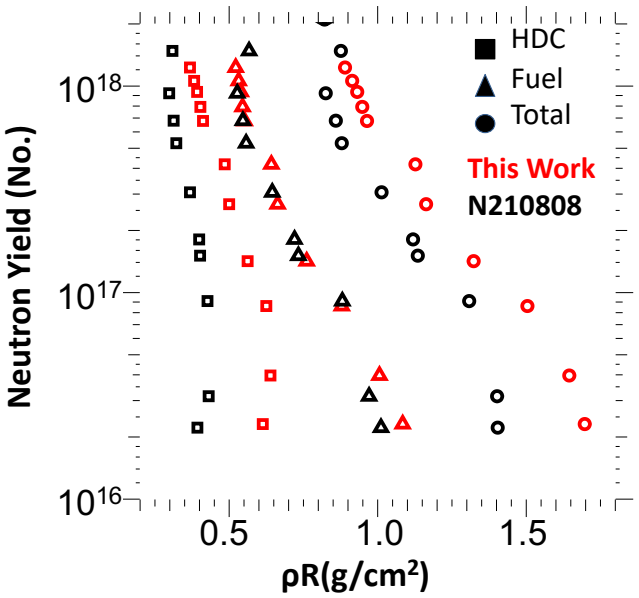

FIG. 7. Calculated neutron yield as a function of areal density (taken at time of peak neutron production) of the HDC diamond ablator (squares), DT fuel (triangles) and total (circles) for the N221204 design (red) compared to N210808 (black) from 1D HYDRA simulations. Here, the yield range is sampled by artificially varying the reaction cross sections on these designs. The difference in areal density between the two designs are largest at low yields, α-off and the areal density for both designs is reduced a higher yields as the burn occurs upon expansion when the hot spot and surrounding dense DT shell are larger.

Additional Design Details

The design for N221204 used a higher amount of W dopant in the diamond ablator compared to N210808 which, together with the thicker ablator, improved the calculated stability at the accelerating DT-fuel ablator interface. Improving the stability at this interface, can increase the amount of clean un-mixed DT fuel [**?**] at large radii near the ablator, which improves its piston efficiency to convert implosion kinetic energy to hot spot internal energy and also results in higher burn-up fractions after ignition once the burn wave propagates into the

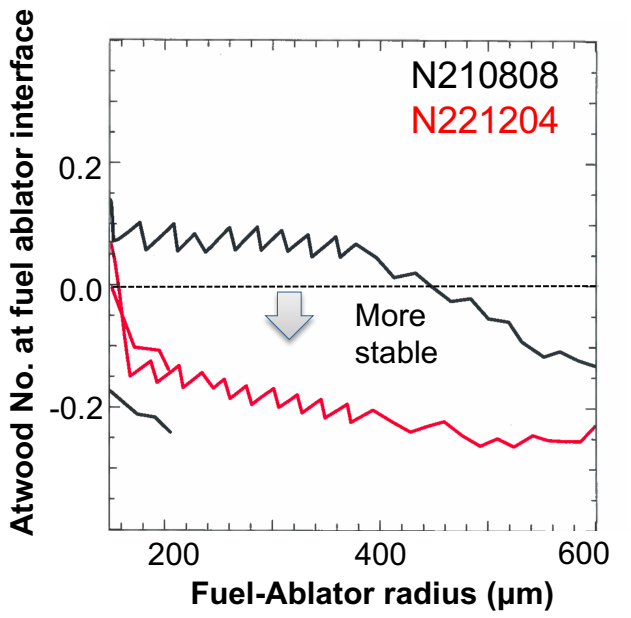

FIG. 8. Calculated Atwood number at the interface between the DT fuel and diamond ablator for N221204 (red curve) compared to N210808 (black curve) as a function of fuel-ablator radius, see the text. For an imploding capsule a lower or more negative Atwood number is more stable to Rayleigh Taylor mixing.

remainder of the DT fuel. For both experiments, the diamond ablators consisted of an inner un-doped diamond layer, a W-doped diamond layer at larger radius (0.44 a.t.%W for N210808 and 0.54-0.6 %W for N221204), and an outer un-doped diamond layer. The crystal structure was nano-crystalline diamond (NCD) for both experiments: N210808 (capsule batch KC789) and N221204 (batch KC952). The total ablator thickness was $\sim$79μm for N210808 and $\sim$85μm for N221204. The target quality for KC952 fielded on N221204 was worse than fielded on N210808, with a greater number of high-Z inclusions in the doped ablator layer [11].

As a result of these design changes, the calculated areal density of the diamond ablator, total (fuel + ablator), and DT fuel at "bang-time" were significantly higher, see Fig. 7 for N221204 (red) compared to N210808 (black). Due to the increase in ablator areal density, we estimate a significant improvement Atwood number for the N221204 design compared to N210808, shown in Fig. 8. The Atwood number is an important parameter to assess the hydrodynamic stability of a design to Rayleigh-Taylor (RT) at material interfaces, defined as $A = (\rho_1 - \rho_2)/(\rho_1 + \rho_2)$, where ρ_1 is the density of the compressed DT fuel and ρ_2 is the density of the remaining ablator material. When this parameter is smaller or negative the accelerating fuel-ablator interface is more stable, reducing growth of the RT instability. In addition the thicker ablator provided a better in-flight aspect ratio (IFAR=radius/thickness measured at the time of peak acceleration) and a longer distance for perturbations to travel to feed through and impact the implosion.

Energy Balance

The energy balance of incident laser light into the hohlraum and implosion were estimated using HYDRA 2D simulations calibrated to experimental measurements. We estimate that about 54.1% of the incident laser energy is used to heat the hohlraum wall (of that $\sim$ 4.4% is deposited in the gold lining and $\sim$ 49.7% in the depleted uranium wall), 25.2% of the incident laser energy becomes radiation loss out of the laser entrance holes, 4.5% of the incident laser energy is used to heat the Helium gas fill in the hohlraum, and $\sim$16.2% is absorbed by the capsule. In addition to these terms, to match experimental data, the laser energy needs to be degraded in simulations by 9-13%. Then, the useful energy coupled to the implosion (and not in the ablated capsule material) is $\sim$246 kJ or $\sim$12%. The fuel kinetic energy is $\sim$15.33 kJ, and the total work done on the DT fuel is $\sim$20kJ (1% of the laser energy). Of this work, $\sim$ 8.2 kJ is coupled to hot spot internal energy.

Symmetry optimization

The first attempt to field the new design (N220919) displayed oblate symmetry of $\sim$12μm in the primary neutron image which provides a picture of the hot spot plasma shape. This was in-part due to a maximum limit on the wavelength separation, which increases transfer from the "outer" to "inner" beams, that could be fielded on the first test due to concerns with laser damage from back-scattered laser light via Stimulated Brillouin Scattering (SBS). However, even with this level of hot spot oblateness, the new design resulted in a fusion energy $>$ 1 MJ (1.22 MJ, $\sim 4.32x10^{17}$ total neutron yield) due to increased margin for robustness to perturbations, but was significantly lower than the full design potential with good symmetry. Two dimensional simulations of this experiment (2D "Total degradation", see the Appendix) predicted that improving the symmetry could lead to $>$ 2x increase in fusion energy yield, see Fig. 5.

The simulations with similar hot spot shape but more symmetric dense DT fuel shape give higher yield for a given level of hot spot P2. The asymmetric dense DT fuel shape is caused by fluctuations in the time-dependent radiation drive symmetry. These fluctuations will be directly interrogated via x-ray radiography of the in-flight shell shape earlier in the implosion history, in separate tuning experiments. If the higher-fluctuation cases are experimentally verified, efforts to further optimize im-

plosion symmetry will continue and should significantly improve the yield. If the lower-fluctuation cases (higher yield) are experimentally verified, the difference in yield between the simulations and N221204 could be attributed to known diamond capsule defects present in these experiments [11], which will also be tested in future experiments fielding higher quality diamond capsules.

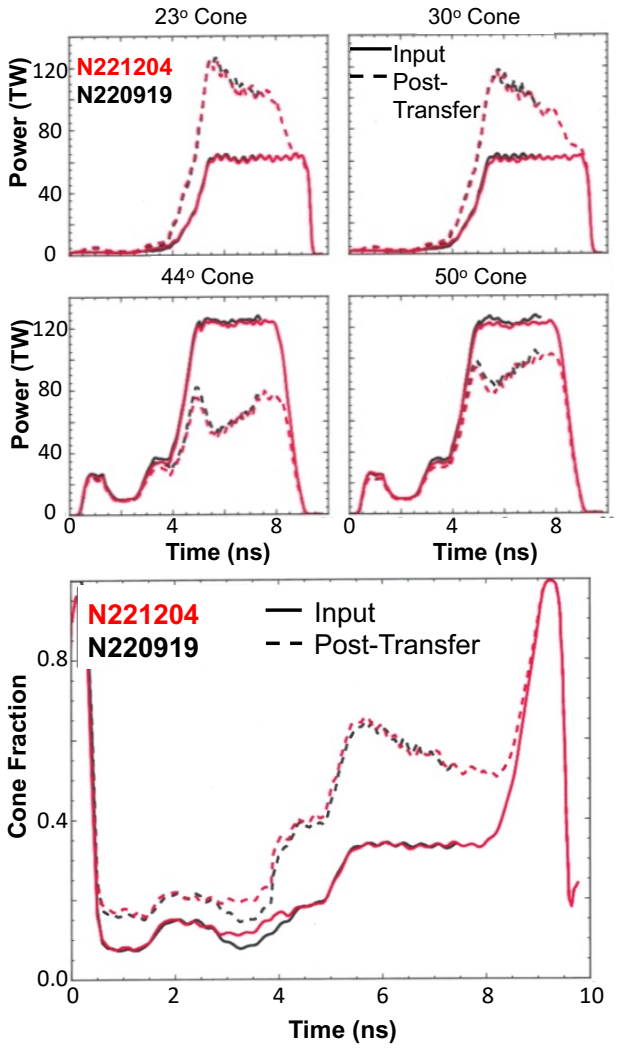

FIG. 9. Changes made to the input laser pulse to reach target gain >1 following the first new design attempt N220919 (1.22MJ) and N221204 (3.15 MJ). (top) The amount of transfer was increased for N221204 (red) compared to N220919 (black) via increasing ($\Delta\lambda$) from 2.5$\AA$ to 2.75$\AA$. The input laser powers (solid lines) and calculated laser powers (dashed lines) are shown for all cones post-energy transfer for N221204 (red) vs N220919 (black). (bottom) The requested input cone fractions (solid lines) were also adjusted, ratio of the "inner" cone power to total laser power, to optimize the time-dependent symmetry based on the updated hohlraum model (see Simulation Methodology of the Appendix). The post-transfer cone fractions (dashed lines) are shown for N221204 (red) vs N220919 (black).

The hot spot symmetry improvement was the only

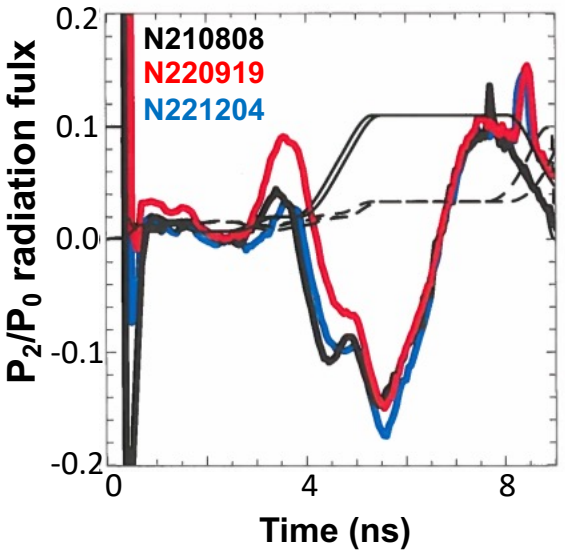

FIG. 10. Mode 2 of the simulated Legendre decomposition of the radiation flux asymmetry (P2/P0) for N210808 (black) N220910 (red) and N221204 (blue) plotted together with the scaled requested laser power as a function of time (solid black lines), and cone fraction (ratio of "inner" laser cones to total power) as a function of time (dashed lines). The P2 decomposition is within the specification during the "foot", until the rise to peak power, but is allowed to swing during the peak of the pulse (see the text). Values of P2/P0 < 0 have higher radiation temperature at the waist of the hohlraum.

change between N220919 (P2=-12μm) and N210808 (P2=$\sim$0μm) accomplished by adjusting the laser input conditions to achieve a symmetric radiation drive surrounding the capsule early in the pulse and swinging the inner drive a little higher to account for the later-time reduction in inner waist drive as the hohlraum plasma fills. To increase drive at the waist of the hohlraum during the peak of the pulse, the amount of laser power transferred from the "outer" to "inner" beams (Cross-beam-energy-transfer, CBET) was increased by increasing the wavelength detuning ($\Delta\lambda$="Inner" beam - "Outer" beam before laser frequency tripling) [21–24] from $\Delta\lambda = 2.5\AA$ for N210919 to $\Delta\lambda = 2.75\AA$ for N221204. Since late-time laser beam propagation through the plasma filled hohlraum is difficult to model, a data-driven model (Callahan, *et al.*) [28] was used together with an experimental sensitivity curve hot spot P2 vs $\Delta\lambda$ to set the optimal wavelength separation for N221204, see also Kritcher *et al.* [9]. We also use simulations to predict changes in symmetry from prior experiments, such as the impact of the extra diamond ablator payload on symmetry. The additional transfer can be seen in Fig. 9 (top) which shows the pre and post-CBET transfer powers on all four laser cones (inner: 23° & 23° and outer: 44° & 50° cones). Figure 9 (bottom) shows the pre and post-CBET cone fraction (ratio of power on the inner cone to

total power) for N221204 vs N210808.

The intentional increase in energy transfer during the peak of the pulse also results in more transfer during the "foot" of the pulse (before the rise to peak power) which was then re-optimized by adjusting the time-dependent foot cone fraction [23, 54, 56](ratio of power on the inner cone to total power), see Fig. 9 (bottom). Typically as the transfer is turned up in the peak, the optimal early time cone-fraction (before 4.5 ns) is turned down to account for the additional transfer in achieving optimal time-dependent symmetry. However, here the cone fraction was increased for N221204 compared to N220919 even with a large amount of CBET to respond to shock symmetry data taken directly before this experiment (N221106), which showed a smaller asymmetry in the foot at lower wavelength separations for prior tuning experiments. The hohlraum model was adjusted to this data by modifying the CBET saturation, and gave a better extrapolation for foot symmetry tuning at higher wavelength separation. This new model was verified in a shock timing experiment (N230110) following N221204 which enabled tuning a symmetric "foot" leading to lower asymmetries in the compressed fuel ρR.

Cross-beam-energy-transfer is used to control the symmetry instead of varying the peak laser power between the cones, to enable using maximum energy of the NIF laser. Controlling the symmetry by varying laser power alone would require reducing the outer beam power to 150-200TW from a maximum 440 TW at 2.05 MJ, foregoing the benefit of increased laser energy.

Given these changes in wavelength detuning and input cone fractions, the resulting post-transfer change to the mode two Legendre moment of the radiation flux asymmetry is shown in Fig. 10 for N220919 vs N221204, compared to N210808. Also shown are the scaled laser pulses and cone fractions as a function of time. Since the outers are "drooping", or ramping down, late in time while the "inner" beams are being held on, this causes the late time increase in cone fraction. This "drooping" was incorporated into the design to enable using the full NIF energy and power on all 192 laser beams, increase the late-time ablation pressure, and mitigate potential laser backscattering out of the hohlraum late in time from the "outer" beams which interact with the high Z expanding wall plasma. The cone fraction in the peak (33%) was also chosen (together with the shape of the droop) to enable the full use of NIF at maximum power. This results in a swing in the temporal P2 flux asymmetry during the peak of the pulse which transitions from being higher temperature at the waist to higher temperature at the poles as the wall ingresses and blocks the inner beams from reaching the center of the hohlraum. If this swing can be balanced the imploding shell and hot spot symmetry can be maintained.